Biosensors and Bioelectronics 133 (2019) 32–38

Contents lists available at ScienceDirect

Biosensors and Bioelectronics

journal homepage: www.elsevier.com/locate/bios

Mimic peroxidase-transfer enhancement of photoelectrochemical aptasensing via CuO nanoflowers functionalized lab-on-paper device with a controllable fluid separator

Jianli Sun[a], Li Li[a], Qingkun Kong[a], Yan Zhang[a,b], Peini Zhao[a,*], Shenguang Ge[c], Kang Cui[a,*], Jinghua Yu[a]

[a] School of Chemistry and Chemical Engineering, University of Jinan, Jinan 250022, PR China
[b] School of Materials Science and Engineering, University of Jinan, Jinan 250022, PR China
[c] Institute for Advanced Interdisciplinary Research, University of Jinan, Jinan 250022, PR China

ARTICLE INFO

Keywords:
Lab-on-paper device
CuO
Photoelectrochemical
Adenosine 5′-triphosphate

ABSTRACT

Inspired by the design of folding greeting cards and tissue drawing covers, a photoelectrochemical (PEC) lab-on-paper device with a controllable fluid separator, producing both reaction zone and detection zone, was explored for ultrasensitive detection of adenosine 5′-triphosphate (ATP) via mimic peroxidase-transfer enhancement of photocurrent response. To realize it, the DNA1, aptamer, and DNA2 as well as the mimic peroxidase of G-quadruplex/hemin modified Au nanocubes were linked on the graphene oxide-functionalized reaction zone via the DNA hybridization. Meanwhile, three-dimensional CuO nanoflowers (CuO NFs) as a photoactive material with outstanding electron transfer ability and absorption of light were grown in situ on the detection zone, providing a PEC active interface. Besides, an innovative fluid separator was elaborately designed by assembling a strip of paper with a hydrophilic channel, providing an effective way to bridge the gap between the two zones with a controllable drawing way, which could successfully avoid the signal interference caused by modifying biomolecules layer by layer on photosensitive materials. In the presence of ATP, the G-quadruplex/hemin modified in the reaction zone was dissociated due to the specific recognition of ATP with aptamer and released into the detection zone with the assistance of controllable fluid separator. The free G-quadruplex/hemin could catalyze hydrogen peroxide to generate oxygen for the consumption of photo-induced electrons from CuO NFs, which could further promote the electron-hole carriers separation efficiency, and eventually resulting in the enhancement of PEC signal. The proposed PEC lab-on-paper device could be employed for specific detection of ATP in the range from 5.0 to 3.0×10^3 nM with a detection limit of 2.1 nM.

1. Introduction

As a newly emerging analytical method, the photoelectrochemical (PEC) techniques combining optical and electrochemical process have attracted considerable research interest due to its desirable performances compared with conventional technologies, such as electrochemiluminescence (Baek et al., 2018; Borducchi et al., 2018; Douman et al., 2017), electrochemical (R. Yang et al., 2018; J. Yang et al., 2018), surface enhanced Raman scattering (Cheng et al., 2017), and fluorescent microarray technology (Peng et al., 2018; Ricciardi et al., 2015). Typically, it possessed intrinsic signal transforming modality, which could convert excitation light into electricity output, leading to significant decrease of background noise signals (Gao et al., 2018; Hun et al., 2018; Niu et al., 2017). So far, to obtain excellent photocurrent response, most researchers have strongly focused on PEC amplification based on the hybrid structure by immobilizing the signal amplified probe on semiconductor material (Kong et al., 2018; Yan et al., 2016; J. Yang et al., 2018; R. Yang et al., 2018; Zhang et al., 2018a; Zhuang et al., 2015). However, it is inevitable to increase the resistance of sensing interface as more and more signal amplified elements are modified, resulting in the decrease of sensitivity (Hao et al., 2018; Liu et al., 2018b). Therefore, exploring innovative signal amplification strategies for avoiding the signal interference caused by the layer-by-layer modification of biomolecules is of urgent needed.

To date, many efforts have been made to develop the easy-to-operate platform, combined with various technologies, for diagnostic tests

* Corresponding authors.
E-mail addresses: chm_zhaopn@ujn.edu.cn (P. Zhao), chm_cuik@ujn.edu.cn (K. Cui).

https://doi.org/10.1016/j.bios.2019.02.027
Received 3 December 2018; Received in revised form 25 January 2019; Accepted 11 February 2019
Available online 19 February 2019
0956-5663/

with the merits of disposable, biocompatible, and high sensitivity (Huang et al., 2018; Jalal et al., 2017; Verma et al., 2018; Zhao et al., 2018). Especially, since the Whitesides' group first reported three-dimensional fluidic devices in 2007, the lab-on-paper device, as an affordable and easy-to-use platform, has been greatly applied in point-of-care diagnosis with PEC technology (Desmet et al., 2016; Liu et al., 2012; Zhang et al., 2018b; Li et al., 2018). For instance, an origami paper-based electrophoretic device was presented for rapid protein separation by unfolding the origami paper and cutting out desired layers, which were more conducive to the regulation and control of fluids on the surface of paper (Luo et al., 2014). Combined with wax printing technology to build a reconfigurable switch by cutting a channel into two parts, where the fluid flow of the lab-on-paper device could be generated along the hydrophilic channel without the need of external pumps or other power supplies (Li et al., 2017). On the basis of these studies, the paper-based sensing platform with different working unites was designed innovatively, which could solve the steric hindering problem in the process of modifying biomolecules layer by layer on photosensitive materials. The construction of the fluid separator as a controllable switch further improved the smooth implementation of this multi-module microfluidic device.

The P-type-semiconductor-based photoactive materials feature great potential of anti-interference capability and intriguing PEC properties for its larger affinity toward electron acceptors (Dai et al., 2017; Kolay et al., 2017; Zheng et al., 2016). Among them, copper oxide (CuO)-based nanomaterials have proved to be an excellent electrode material with attractive narrow bandgap semiconductor (1.7 eV) that can effectively harvest photon energy across the visible light spectrum and promote the separation of photo-generated electron-hole pairs, resulting in noticeably increased photocurrent (Karim et al., 2018; Zhang et al., 2018a, 2018b; Zhu et al., 2017). In particularly, three-dimensional CuO nanoflowers (CuO NFs) showed more prominent electron transfer ability and absorption of light than that of 1D or 2D structures, including nanotubes, nanowires, and nanobranches (Chen et al., 2018; Klein et al., 2016; Yuan et al., 2014). As is well-known, the spatial distribution is core factor which impacts the physical or chemical properties of photosensitive material greatly (Morbioli et al., 2017). Thus, the assembling of CuO NFs on substrates with three-dimensional porous structure such as cellulose paper is a promising candidate for realizing signal amplification in PEC analysis.

Herein, a novel PEC lab-on-paper device with a fluid separator was constructed for ultrasensitive detection of adenosine 5′-triphosphate (ATP) via mimic peroxidase-transfer enhancement of photocurrent response. In the reaction zone of the lab-on-paper device, the G-quadruplex/hemin could be dissociated by the appearance of ATP and transported to the detection zone functionalized by CuO NFs through a controllable fluid separator. Under the light irradiation, the CuO NFs exhibited the excellent PEC performance with improvement of visible light absorption and the PEC intensity. In this work, the innovative design of distributing the signal probe and photoactive material in different working unites connected by a fluid separator on lab-on-paper device could efficiently reduce signal interference. The proposed PEC platform presented high sensitivity and selectivity for the determination of ATP, and had a wide linear range compared with other analytical methods.

2. Experimental section

2.1. Design of the lab-on-paper device

Inspired by the design of folding greeting and tissue drawing covers in daily life, a lab-on-paper device was established for the determination of ATP, and the specific size of paper was designed by using Adobe illustrator CS6 software (Scheme 1A and B). As illustrated in Scheme 1C, the unique device was composed of a waste collection tab (red), a reaction tab (green), a detection tab (blue), an electrode tab (purple), and a fluid separator (20.0 mm × 3.0 mm) with the hydrophilic channel (3.0 mm × 2.0 mm). On the reaction tab, a circular hydrophilic region with a diameter of 7.0 mm was designed as reaction zone and could be cut along the cutting line. In addition, a hollow channel (3.0 mm × 2.0 mm) was designed in the detection tab to facilitate fluid flow to the detection zone. When the device was folded together, the fluid in the two separate tabs would be connected by the fluid separator. Moreover, to achieve the automation of rinse steps, a rectangular fluid reservoir (16.0 mm × 8.0 mm) was introduced into the waste collection tab, which could efficiently avoid contamination of reagents in the operation process. Finally, the hydrophilic circular zone (7.0 mm in diameter) on the electrode tab was used to print the carbon counter electrode and Ag/AgCl reference electrode (Scheme 1D), and the carbon working electrode was printed on the back of the detection zone (Scheme 1E).

2.2. Assembly and assay procedures of the lab-on-paper device

The analytical procedures of the lab-on-paper device are shown in Fig. 1. (i) To obtain an ideal amplified PEC signal, CuO NFs/rGO conductive substrate was introduced into the detection zone, where the excellent PEC properties of CuO NFs were beneficial for effectively extending the range of linear detection in the analysis process (Fig. 1A). In detail, the reduced graphene oxide (rGO, 2.0 μL) was added to the detection zone of the paper device and used as the conductive substrate. Subsequently, CuO NFs grown on rGO conductive cellulose fibers by in-situ synthesized method provided a favorable optimal photosensitive material in PEC signal amplify process. (ii) The sensing interface in the reaction zone was established by modifying specific DNA sequences (The sequences were listed in Table S1). DNA1 was first immobilized on the GO substrate, and then the aptamer and signal probe were modified to its surface through the hybridization reaction (Fig. 1B). Concretely, GO aqueous solution (2.0 μL) was dropped onto the reaction zone of the device, the carboxylic groups of GO film were activated in 10 mM 1-ethyl-3-(3-(dimethylamino)propyl) carbodiimide (EDS) and 20.0 mM N-hydroxysulfosuccinimide (NHS) solutions for 45 min. Afterward, 20.0 μL of DNA1 (0.1 μM) was added to its surface and incubated for 12 h at 4 °C. After the reaction zone was washed thoroughly to remove the unlinked DNA1, 20.0 μL of aptamer (40.0 nM) was dropped on the surface to incubate for 45 min at 37 °C. The unbound or physically adsorbed molecules were rinsed with washing buffer solution (PBS, pH 7.4). Nonspecific active sites were blocked with 20.0 μL of 1% bovine serum albumin (BSA) for 45 min at room temperature. Subsequently, the modified zone was injected into 20.0 μL of signal probe (DNA2-Au NCs-G-quadruplex/hemin, the detailed synthesis method was listed in the Supporting Information) to react for 30 min at 37 °C and thoroughly washed with PBS to remove unhybridized signal probe. (iii) To realize the accurate sensing system with easy operation, the liquid wastes need to be treated urgently by folding the waste collection tab along the designed dotted line (Fig. 1C). When the washing buffer was added to the reaction zone, unbound or physically adsorbed molecules could flow to the waste collection zone through a hydrophilic channel. (iv) To carry out the biological reactions, 20.0 μL of different concentrations of ATP was incubated for 80 min on the reaction zone at 37 °C, which led to the release of signal probe and transfer from the reaction zone to the detection unit when the fluid separator acted as a bridge for fluid transmission between two regions (Fig. 1D and E). (v) After 20.0 μL H_2O_2 (1.5 mM) was added to the detection zone in the absence of the fluid separator, O_2 gas was rapidly generated under the catalysis of G-quadruplex/hemin, resulting in a large amount of electrons consumption of CuO NFs under the light irradiation, which was favorable for increasing the PEC signal (Fig. 1F). Finally, the ideal PEC signal was collected with the utilization of CHI 660D electrochemical workstation at applied potential of 0 V. (Fig. 1G and H). Such a signal enhancement mainly originated from the synergistic effect between CuO and G-quadruplex/hemin. The possible mechanism of catalytic reaction might

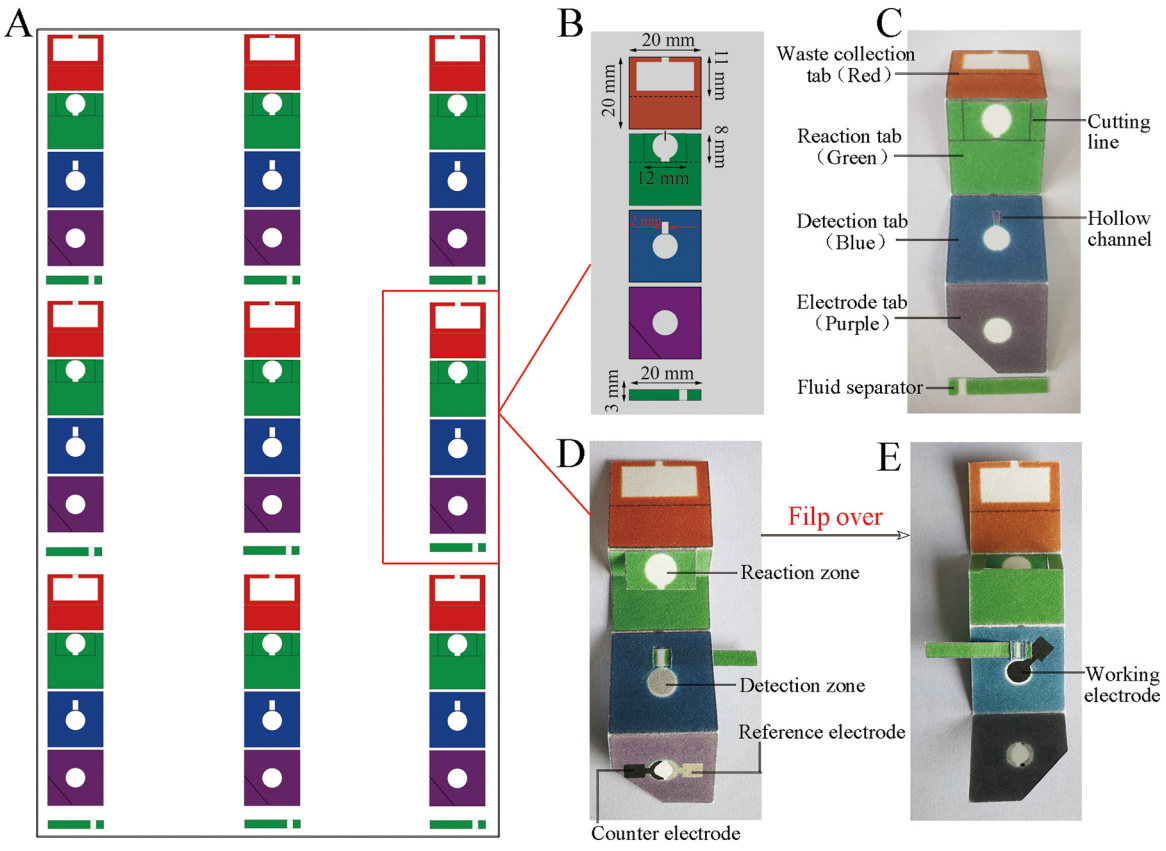

Scheme 1. (A-E) Schematic layout and shape of the fabricated lab-on-paper device with screen-printed electrodes.

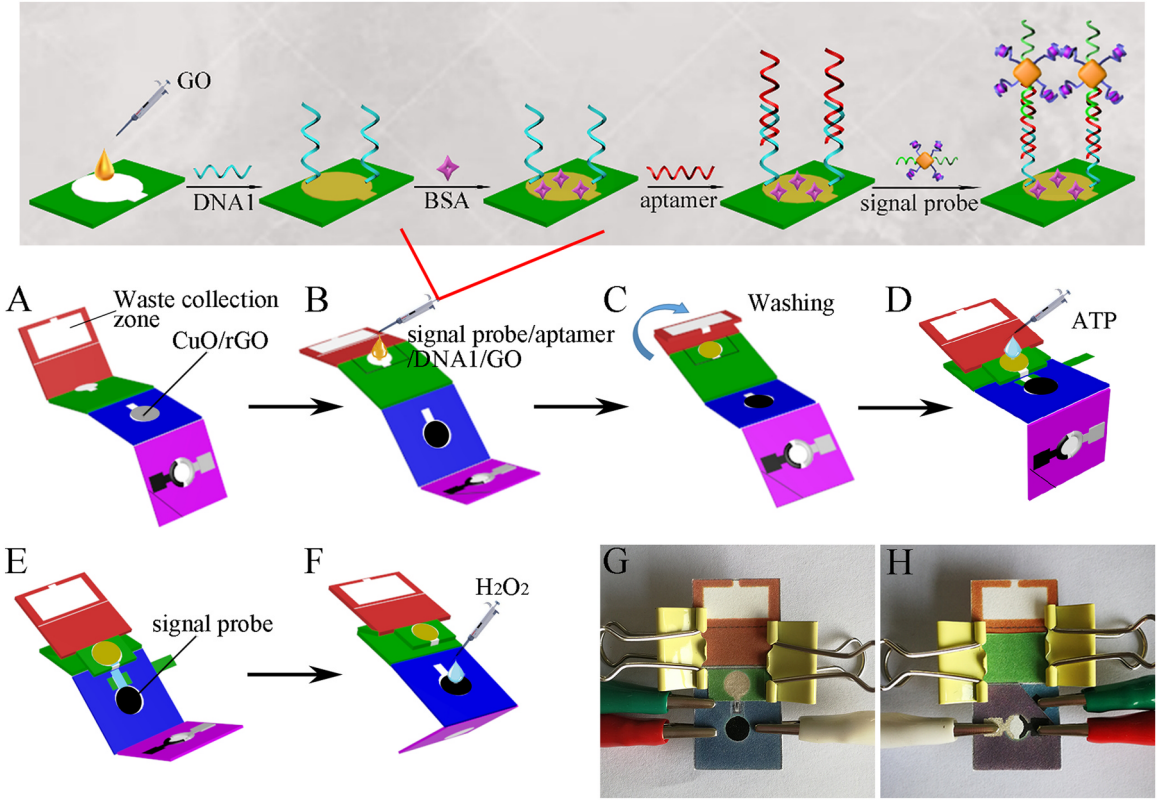

Fig. 1. (A-F) Assay procedures and (G and H) photographs of the lab-on-paper device.

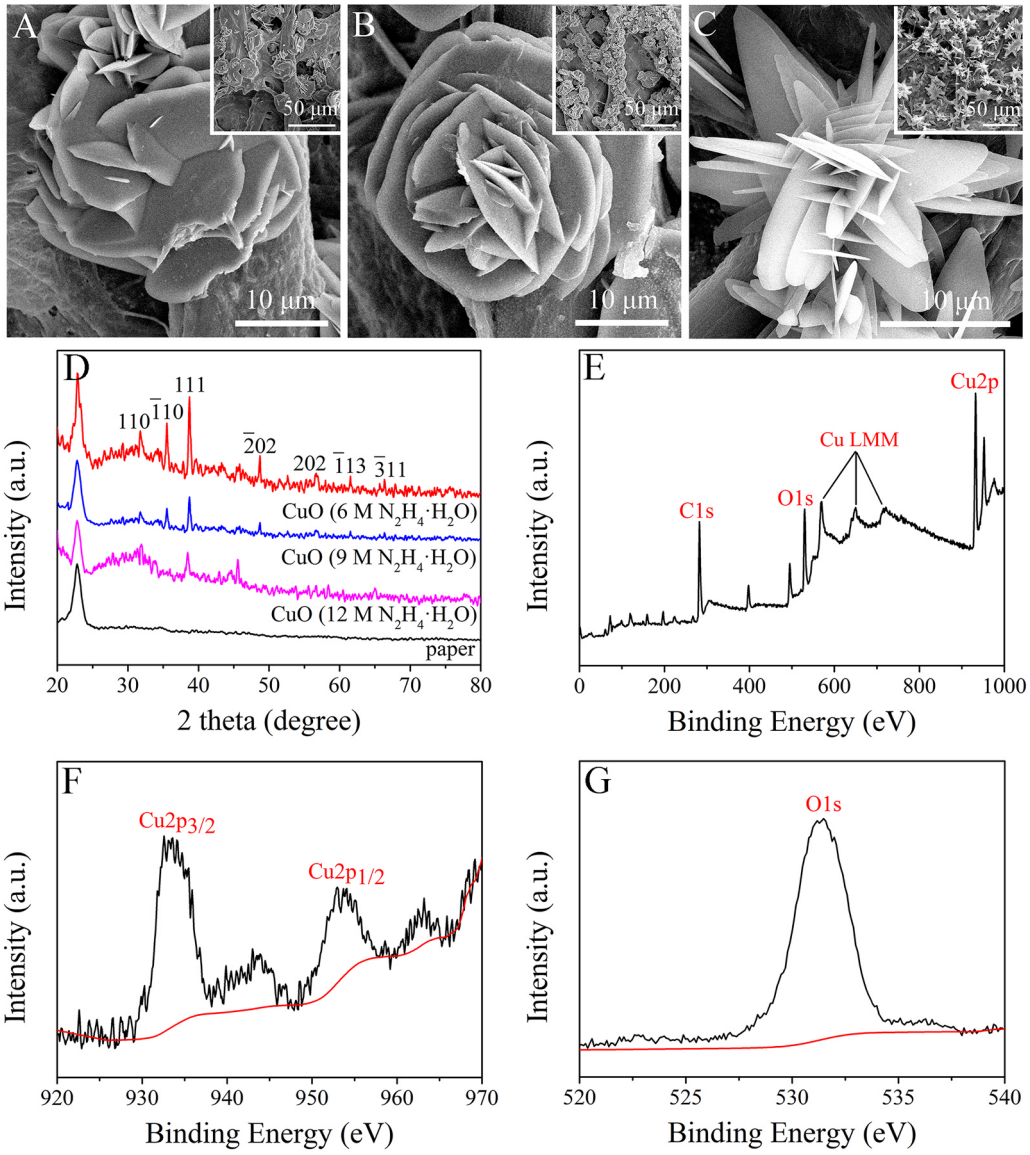

Fig. 2. (A-C) SEM images of the CuO NFs synthesized by adding different concentrations of $N_2H_4{\cdot}H_2O$ solution. (D) XRD patterns of the as-prepared CuO NFs. (E) XPS spectra of CuO NFs (6 M $N_2H_4{\cdot}H_2O$) wide scan, (F) high resolution Cu2p region and (G) high resolution O1s region.

be depicted as follows (Lu et al., 2008; Tang et al., 2014; Xuan et al., 2012).

$$\text{hemin[Fe(III)]} + H_2O_2 \rightarrow \text{hemin[Fe(IV)} = O^{\cdot+}\text{]} + H_2O \quad (1)$$

$$\text{hemin[Fe(IV)} = O^{\cdot+}\text{]} + H_2O_2 \rightarrow \text{hemin[Fe(III)]} + H_2O + O_2 \quad (2)$$

3. Results and discussion

3.1. Characterization of CuO NFs grown on rGO-modified cellulose

To further achieve the amplification of PEC signal, the conductive material rGO was modified on the detection zone. When rGO solution was dropped onto the cellulose paper, the thin and transparent rGO layer was produced as a flexible layer firmly attached onto cellulose fibers (Fig. S2B). Compared with the pure cellulose paper (Fig. S2A), it could be clearly seen that the pores of paper were blocked due to the successful modification of rGO on paper, which proved the formation of conductive substrate. To obtain the optimal PEC response, CuO modified rGO/cellulose with different morphologies were synthesized by regulating the reductant concentration during the growth process. The SEM images of Fig. 2 showed that the concentration of hydrazine hydrate ($N_2H_4{\cdot}H_2O$) was an important influencing factor for CuO morphology and performance. When the concentration of $N_2H_4{\cdot}H_2O$ was 12 M, the growth of CuO was nonuniform and the shape of the petals was irregular (Fig. 2A). As the concentration of $N_2H_4{\cdot}H_2O$ decreased within a certain range, CuO nanosheets grown on the surface of rGO became slightly denser. As displayed in Fig. 2B, a large amount of nanosheets were cross-linked as petals and assembled into a hierarchical nanostructure that grew on the rGO surface. Moreover, the flowerlike structure was composed of 10 μm nanosheets with relatively smooth surface when the $N_2H_4{\cdot}H_2O$ concentration was 6 M (Fig. 2C), indicating that CuO NFs were supported on rGO with a uniform distribution during the whole growing process. Besides, Cu and O elements were presented in the energy-dispersive spectroscopy (EDS) patterns (Fig. S3A). The corresponding mapping showed that both Cu and O elements distributed uniformly throughout the cellulose paper (Fig. S3B and S3C), which confirmed that the CuO NFs was successfully formed on rGO modified cellulose.

In addition, X-ray diffraction (XRD) characterization was performed to determine the crystal structure of CuO NFs. It can be observed that the change of phases intensity was obvious as the concentration of the

$N_2H_4{\cdot}H_2O$ varied from 6 M to 12 M. As shown in Fig. 2D, the XRD pattern showed the Bragg's reflections at 32.5, 35.5, 38.7, 48.7, 58.2, 61.3, 66.1°, which correspond to the (110), (_111), (111), (_202), (202), (_113), (_311) planes (JCPDS No.45–0937), respectively. Furthermore, CuO NFs had the best crystal structure with the usage of 6 M $N_2H_4{\cdot}H_2O$, indicating that it could be successfully applied in PEC analysis as an optimal photosensitive material.

For further comprehending of photoactive material, XPS analysis was carried out to investigate the elemental compositions and oxidation state of CuO NFs with $N_2H_4{\cdot}H_2O$ concentration of 6 M. As shown in Fig. 2E, the typical XPS wide scan analysis revealed the presence of copper (Cu2p and its Cu LMM Auger), oxygen (O1s) and carbon (C1s) on the surface of nanomaterials. Besides, the Cu2p spectrum exhibited a Cu2p3/2 peak at 933.6 eV and a Cu2p1/2 peak at 953.6 eV along with a series of shakeup satellites peak, thus confirmed the existence of Cu^{2+} on the surface (Fig. 2F). The corresponding high resolution XPS spectrum of the O1s region was shown in Fig. 2G, and the peak appeared at 531 cm^{-1} due to the Cu-O stretching band of CuO NFs. These results significantly demonstrated the successful synthesis of CuO NFs. In addition, PEC experiment was conducted to investigate performance of the three types of CuO NFs, and it could be observed that the CuO synthesized by adding $N_2H_4{\cdot}H_2O$ with a concentration of 6 M had the outstanding PEC response (Fig. S4). Therefore, CuO NFs with $N_2H_4{\cdot}H_2O$ concentration of 6 M was selected as photoactive material for PEC analysis.

3.2. Characterization of signal probe

As shown in Fig. 3A, the SEM image demonstrated the morphology of the synthesized gold nanomaterials, which presented a typical cube–like structure. Moreover, the surface morphology and shape of nanomaterials were observed by TEM, and the size of resulted Au NCs was approximately 95 nm (Fig. 3B). Previous literatures have indicated that Au NCs possessed several characteristics such as biocompatibility, chemical stability, and plasmon tunability, which were more favorable for the attachment of G-quadruplex and DNA2 to become suitable candidate for signal probe construction (Liu et al., 2018a). Therefore, the UV–vis absorption spectra (Fig. 3C) was utilized to characterize the as-synthesized signal probe. It was found that an absorption peak of spectrum appeared at 569 nm (curve a), indicating the successful synthesis of Au NCs. After assembling G-quadruplex and DNA2 on the surface of Au NCs, the obtained composite structure exhibited a typical characteristic absorbance of DNA2 at 310 nm (curve b), and the Au NCs absorption peak underwent a red shift to 585 nm, indicating that they were successfully loaded on Au NCs. When hemin was eventually added into the solution to form the signal probe, absorption peaks occurred at 584 and 336 nm (curve c), demonstrating the successful combination of hemin and G-quadruplex.

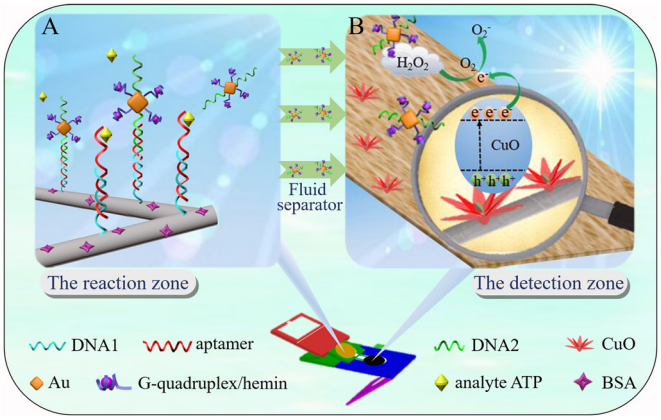

Scheme 2. PEC analytical principle of the lab-on-paper device.

3.3. The working mechanism of the proposed lab-on-paper device

The working principle of the proposed strategy was illustrated in Scheme 2. In the presence of analyte ATP, the dissociation of G-quadruplex/hemin modified in the reaction zone was triggered due to the specific recognition of ATP with aptamer (Scheme 2A). And then the released G-quadruplex/hemin flowed into the detection zone with the assistance of controllable fluid separator. Under the light irradiation, the CuO NFs with preferable morphology growing in situ on the detection zone exhibited the excellent PEC performance, which could tremendously improve visible light absorption and promote the PEC intensity. The free G-quadruplex/hemin could catalyze hydrogen peroxide to generate O_2 for the consumption of photo-induced electrons from CuO NFs, which greatly improved the separation efficiency of electron hole carriers, leading to further amplification of the PEC signal (Scheme 2B) (Dai et al., 2018; Dou et al., 2018). Therefore, the designed lab-on-paper device could be successfully applied to the detection of target ATP through cascade reaction in the PEC analysis process.

3.4. Optimization of experimental conditions

To obtain the optimum performance of the proposed lab-on-paper device for ATP detection, several possible influencing factors including the concentration of aptamer, the incubation times of both signal probe and the ATP, and the concentration of H_2O_2 should be studied. The detailed research process was in the Supporting Information and the results were shown in Fig. S5.

3.5. Analytical performance of lab-on-paper device

It can be seen that the intensity of photocurrent has strong

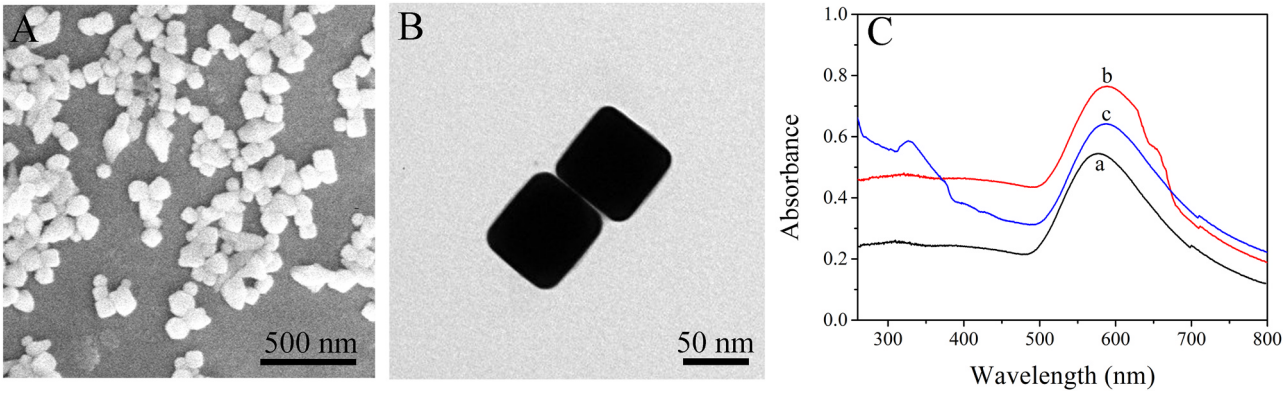

Fig. 3. (A) SEM and (B) TEM images of Au NCs. (C) UV − vis spectra of Au NCs (a), DNA2-Au NCs-G-quadruplex (b), and signal probe (c).

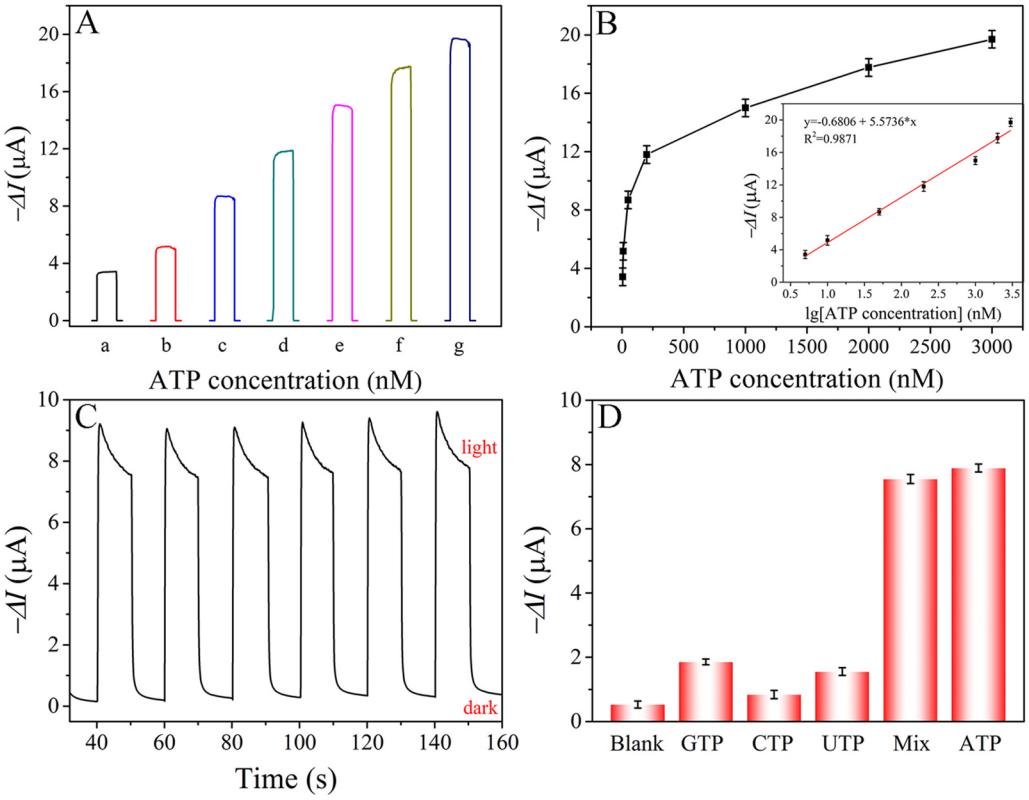

Fig. 4. (A) Photocurrent responses of the device at 5, 10, 50, 200, 1000, 2000 and 3000 nM ATP (from a to g) and (B) the corresponding calibration curve of the photocurrent increment versus ATP concentration. (C) Stability of the PEC sensor incubated in 50 nM ATP under consecutive cyclic potential scans. (D) Selectivity of the proposed device with different interfering targets.

dependence on the concentration of ATP, as shown in Fig. 4A. Under the optimal conditions, the increase of ATP concentration contributed to the improvement of photocurrent response. The signal probes were released from the reaction zone, resulting that more G-quadruplex/hemins could be employed to efficiently catalyze the reduction of H_2O_2 on the detection zone. The calibration plot in Fig. 4B displayed a good linear relationship between photocurrent intensity and the logarithmic value of ATP concentration ranging from 5.0 to 3.0×10^3 nM. The equation of the calibration curve was $\Delta I = 0.6806–5.5736 \lg c$ ($\Delta I = I – I_0$, I_0 was the current response when analytes concentration was zero, c stands for the concentration of ATP, and the correlation coefficient of was 0.9935). The detection limit was estimated to be 2.1 nM at the signal-to-noise ratio of 3. In addition, compared with previous PEC bioanalysis using DNA strands, the lab-on-paper device had relatively wide linear range and low detection limit (Table S2). To investigate the stability of the PEC devices, current-time curve was measured in the presence of 50 nM ATP. As shown in Fig. 4C, the current response decreased to about 96% of its initial value, certifying that the sensor had good long-term stability. The relative standard deviation (RSD) was less than 2.1%, indicating the good stability of the proposed sensor. Moreover, the selectivity and the binding specificity of the proposed PEC sensor were evaluated as shown in Fig. 4D, changes in the photocurrent were performed by the incubation of ATP and other analogues such as CTP, GTP, and UTP. It was obvious that ATP showed higher photocurrent response compared with the other analogues even if their concentrations were 5-fold higher than that of ATP. The PEC intensity obtained from the mixture (50 nM ATP, 1000 nM GTP, 1000 nM CTP and 1000 nM UTP) showed no obvious change when compared with that obtained from pure target ATP. The results implied that the present sensor had excellent selectivity for ATP.

4. Conclusion

In summary, a novel PEC paper-based device has been successfully designed and demonstrated its application in measuring ATP at the point-of-care diagnosis. The signal amplification strategy was achieved using CuO NFs as photoactive materials and aptamer-involved composite structure as the signal switch. Combined with the foldability and hydrophilicity of the paper, the fluid separator was innovatively designed as a controllable switch so that the fluid containing signal probe could flow smoothly from the reaction zone to the detection zone. The conception of separating the modification of biomolecules from the PEC transducer, provided a universal strategy for ultrasensitive monitoring of biomarkers in bioanalysis. More importantly, the developed paper-based ATP sensor exhibited long-term stability, excellent specificity, and fabrication reproducibility. Through continuous development of this system, we envision a non-instrumented, visually readable device that can dramatically improve the efficiency of clinical diagnostic tests in resource-limited setting.

CRediT authorship contribution statement

Jianli Sun: Conceptualization, Methodology, Writing - original draft. **Li Li:** Investigation, Formal analysis. **Qingkun Kong:** Visualization, Data curation. **Yan Zhang:** Resources, Data curation. **Peini Zhao:** Resources, Visualization. **Shenguang Ge:** Supervision, Funding acquisition. **Kang Cui:** Writing - review & editing, Resources. **Jinghua Yu:** Funding acquisition, Project administration.

Acknowledgements

The authors are thankful for support from the National Natural Science Foundation of China (51872121 and 21874055), the program for Taishan Scholar of Shandong Province (ts201712048), and Major Program of Shandong Province Natural Science Foundation (ZR2017ZC0124).

Declaration of interests

None

Appendix A. Supporting information

Supplementary data associated with this article can be found in the online version at doi:10.1016/j.bios.2019.02.027.

References

Baek, S., Kwon, S.R., Yeon, S.Y., Yoon, S.H., Kang, C.M., Han, S.H., Lee, D., Chung, T.D., 2018. Anal. Chem. 90 (7), 4749–4755.

Borducchi, E.N., Liu, J., Nkolola, J.P., Cadena, A.M., Yu, W.H., Fischinger, S., Broge, T., Abbink, P., Mercado, N.B., Chandrashekar, A., Jetton, D., Peter, L., McMahan, K., Moseley, E.T., Bekerman, E., Hesselgesser, J., Li, W., Lewis, M.G., Alter, G., Geleziunas, R., Barouch, D.H., 2018. Nature 563 (7731), 359–361.

Chen, X., Chu, D., Wang, L., Hu, W., Yang, H., Sun, J., Zhu, S., Wang, G., Tao, J., Zhang, S., 2018. J. Mol. Struct. 1157, 337–340.

Cheng, Z., Choi, N., Wang, R., Lee, S., Moon, K.C., Yoon, S.Y., Chen, L., Choo, J., 2017. ACS Nano. 11 (5), 4926–4933.

Dai, H., Chen, Y., Niu, X., Pan, C., Chen, H., Chen, X., 2018. Biosens. Bioelectron. 118, 36–43.

Dai, W.X., Zhang, L., Zhao, W.W., Yu, X.D., Xu, J.J., Chen, H.Y., 2017. Anal. Chem. 89 (15), 8070–8078.

Desmet, C., Marquette, C.A., Blum, L.J., Doumeche, B., 2016. Biosens. Bioelectron. 76, 145–163.

Dou, B., Yang, J., Yuan, R., Xiang, Y., 2018. Anal. Chem. 90 (9), 5945–5950.

Douman, S.F., Brennan, E., Iwuoha, E.I., Forster, R.J., 2017. Anal. Chem. 89 (21), 11614–11619.

Gao, P., Wang, H., Li, P., Gao, W., Zhang, Y., Chen, J., Jia, N., 2018. Biosens. Bioelectron. 121, 104–110.

Hao, N., Hua, R., Chen, S., Zhang, Y., Zhou, Z., Qian, J., Liu, Q., Wang, K., 2018. Biosens. Bioelectron. 101, 14–20.

Huang, J.Y., Lin, H.T., Chen, T.H., Chen, C.A., Chang, H.T., Chen, C.F., 2018. ACS. Sensors 3 (1), 174–182.

Hun, X., Li, Y., Wang, S., Li, Y., Zhao, J., Zhang, H., Luo, X., 2018. Biosens. Bioelectron. 112, 93–99.

Jalal, U.M., Jin, G.J., Shim, J.S., 2017. Anal. Chem. 89 (24), 13160–13166.

Karim, M.N., Singh, M., Weerathunge, P., Bian, P., Zheng, R., Dekiwadia, C., Ahmed, T., Walia, S., Della Gaspera, E., Singh, S., Ramanathan, R., Bansal, V., 2018. ACS Appl. Nano. Mater. 1 (4), 1694–1704.

Klein, F., Pinedo, R., Hering, P., Polity, A., Janek, J., Adelhelm, P., 2016. J. Phys. Chem. C. 120 (3), 1400–1414.

Kolay, A., Kokal, R.K., Kalluri, A., Macwan, I., Patra, P.K., Ghosal, P., Deepa, M., 2017. ACS Appl. Mater. Interfaces 9 (40), 34915–34926.

Kong, Q., Cui, K., Zhang, L., Wang, Y., Sun, J., Ge, S., Zhang, Y., Yu, J., 2018. Anal. Chem. 90 (19), 11297–11304.

Li, L., Zheng, X., Huang, Y., Zhang, L., Cui, K., Zhang, Y., Yu, J., 2018. Anal. Chem. 2018. https://doi.org/10.1021/acs.analchem.8b02849.

Li, M.J., Zheng, Y.N., Liang, W.B., Yuan, R., Chai, Y.Q., 2017. ACS Appl. Mater. Interfaces 9 (48), 42111–42120.

Liu, X.P., Chen, J.S., Mao, C.J., Niu, H.L., Song, J.M., Jin, B.K., 2018b. Biosens. Bioelectron. 116, 23–29.

Liu, H., Xiang, Y., Lu, Y., Crooks, R.M., 2012. Ange. Chem. Int. Ed. 51 (28), 6925–6928.

Liu, B., Zhang, D., Ni, H., Wang, D., Jiang, L., Fu, D., Han, X., Zhang, C., Chen, H., Gu, Z., Zhao, X., 2018a. ACS Appl. Mater. Interfaces 10 (1), 21–26.

Lu, X.B., Zhou, J.H., Lu, W., Liu, Q., Li, J.H., 2008. Biosens. Bioelectron. 23, 1236–1243.

Luo, L., Li, X., Crooks, R.M., 2014. Anal. Chem. 86 (24), 12390–12397.

Morbioli, G.G., Mazzu-Nascimento, T., Milan, L.A., Stockton, A.M., Carrilho, E., 2017. Anal. Chem. 89 (9), 4786–4792.

Niu, K., Li, Y., Bai, R., Qu, Y., Song, Y., 2017. J. Mater. Chem. B. 5, 5145–5151.

Peng, Y., Li, D., Yuan, R., Xiang, Y., 2018. Biosens. Bioelectron. 105, 1–5.

Ricciardi, S., Frascella, F., Angelini, A., Lamberti, A., Munzert, P., Boarino, L., Rizzo, R., Tommasi, A., Descrovi, E., 2015. Sens. Actuators, B: Chem. 215, 225–230.

Tang, Y.J., Guo, Y.J., Zhang, L., Cai, J.Y., Yang, P.H., 2014. Biosens. Bioelectron. 54, 628–633.

Verma, M.S., Tsaloglou, M.N., Sisley, T., Christodouleas, D., Chen, A., Milette, J., Whitesides, G.M., 2018. Biosens. Bioelectron. 99, 77–84.

Xuan, J., Jia, X.D., Jiang, L.P., Abdel-Halim, E.S., Zhu, J.J., 2012. Bioelectrochem 84, 32–37.

Yan, Z., Wang, Z., Miao, Z., Liu, Y., 2016. Anal. Chem. 88 (1), 922–929.

Yang, J., Wu, Y., Gan, C., Yuan, R., Xiang, Y., 2018. Biosens. Bioelectron. 117, 743–747.

Yang, R., Zou, K., Li, Y., Meng, L., Zhang, X., Chen, J., 2018. Anal. Chem. 90 (15), 9480–9486.

Yuan, S., Huang, X.L., Ma, D.L., Wang, H.G., Meng, F.Z., Zhang, X.B., 2014. Adv. Mater. 26 (14), 2273–2279.

Zhang, N., Ruan, Y.F., Zhang, L.B., Zhao, W.W., Xu, J.J., Chen, H.Y., 2018b. Anal. Chem. 90 (3), 2341–2347.

Zhang, Y., Xu, R., Kang, Q., Zhang, Y., Wei, Q., Wang, Y., Ju, H., 2018a. ACS Appl. Mater. Interfaces 10 (37), 31080–31087.

Zhang, Y., Zhang, L., Cui, K., Ge, S., Cheng, X., Yan, M., Yu, J., Liu, H., 2018b. Adv. Mater. 2018, 1801588.

Zhang, L., Zhu, Y.C., Liang, Y.Y., Zhao, W.W., Xu, J.J., Chen, H.Y., 2018a. Anal. Chem. 90 (8), 5439–5444.

Zhao, X., Zhao, Y., Zhang, L., Ma, X., Zhang, S., Zhang, X., 2018. Anal. Chem. 90 (3), 2070–2078.

Zheng, Y.N., Liang, W.B., Xiong, C.Y., Yuan, Y.L., Chai, Y.Q., Yuan, R., 2016. Anal. Chem. 88 (17), 8698–8705.

Zhu, Y., Xu, Z., Yan, K., Zhao, H., Zhang, J., 2017. ACS Appl. Mater. Interfaces 9 (46), 40452–40460.

Zhuang, J., Lai, W., Xu, M., Zhou, Q., Tang, D., 2015. ACS Appl. Mater. Interfaces 7 (15), 8330–8338.